Electronic Supplementary Material (ESI) for Journal of Materials Chemistry C.

Supplementary document for

In-situ growth of ultra-smooth or super-rough thin films by suppression of vertical or horizontal growth of surface mounds

Chaoquan Hu*, Jize Cai, Yuankai Li, Chaobin Bi, Zhiqing Gu, Jiaqi Zhu*, Jianfeng Zang* and Weitao Zheng*

*Corresponding authors. (Chaoquan Hu) E-mail: cqhu@jlu.edu.cn; (Jiaqi Zhu) E-mail: zhujq@hit.edu.cn; (Jianfeng Zang) E-mail: jfzang@hust.edu.cn; (Weitao Zheng) E-mail: wtzheng@jlu.edu.cn

This PDF file includes:

Supplementary text
Sections 1 to 11
Figures S1 to S25
Tables S1 to S15

Section 1 GIXRD spectra, SAED and HRTEM images for RT40-HfN films

Fig. S1 shows GIXRD spectra, SAED and HRTEM images of RT40-HfN films with different thicknesses (d = 47, 594 and 1423 nm, corresponding to deposition time t = 5, 40 and 160 min). The film maintains the crystal structure of the rocksalt phase throughout the growth process, which is demonstrated consistently by the (111), (200), (220) and (311) diffraction peaks, diffraction rings and plane spacings.

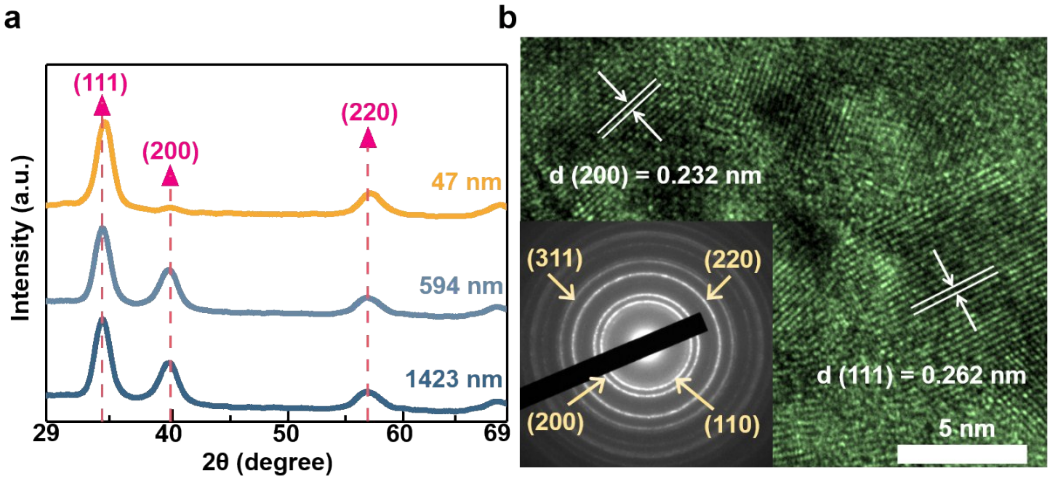

Fig. S1. Structure of RT40-HfN films. a,b, The GIXRD pattern of the HfN films with three film thicknesses of 47 nm, 594 nm and 1423 nm (a) and typical SAED and HRTEM images of the HfN film (b).

Section 2 3D-AFM surface topography, v_R, δ, surface profile and simulation parameters for seven sets of film samples, including Fig.S2-S7, Table S1-S7

Fig. S2-S7 show the 3D-AFM images, roughening rate (v_R), relative vertical-growth coefficient of mounds (δ) and surface profiles for RT10-HfN, HT40-HfN, RT160-HfN, RT240-HfN, RT40-HfN/CN and RT40-HfN-Ag films. The root mean square roughness (R) of the films increases linearly with film thickness (d), indicating that all film samples exhibit a consistent surface roughening behavior during the deposition process. To quantitatively describe the roughening process, v_R was obtained by calculating the slope of the R-d curve. Gwyddion software was used to simulate the surface morphology of film under different protrusion sizes (h, s). By ensuring that the roughness, the slope of the power spectral density (PSD) curves at higher frequencies and the growth exponent (β) obtained by simulation were equal to those obtained by experiment (namely, $R_{Exp} = R_{Sim}$, $k_{Exp} = k_{Sim}$ and $\beta_{Exp} = \beta_{Sim}$), the h and s of each film were determined and $\Delta h/h_0$ and $\Delta s/s_0$ were calculated. δ was obtained by calculating the slope of the $\Delta h/h_0$–$\Delta s/s_0$ curve. The deposition time t, d, R, β, the slope of PSD curves at higher frequencies and simulation parameters of seven sets of film samples (RT10-HfN, RT40-HfN, HT40-HfN, RT160-HfN, RT240-HfN, RT40- HfN/CN and RT40-HfN-Ag) are listed in Table. S1-S7.

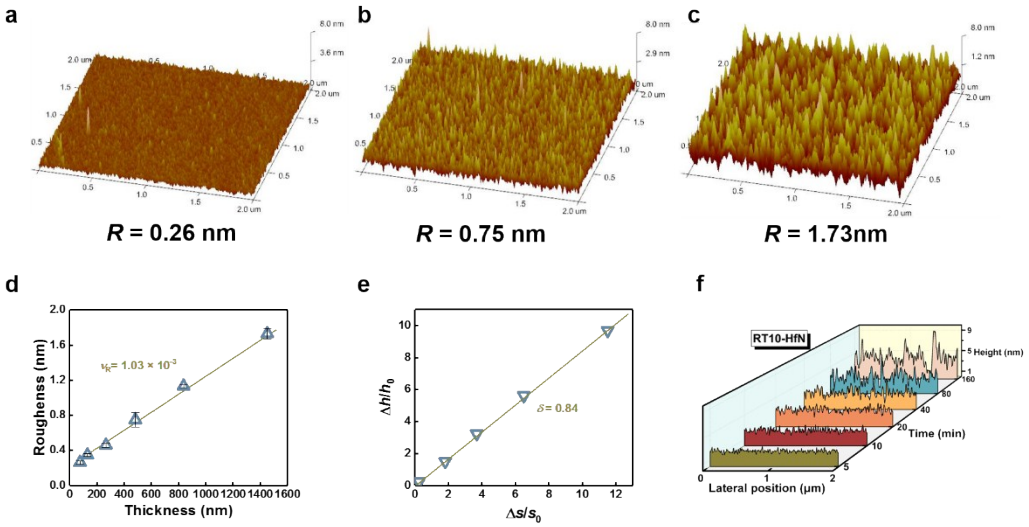

Fig. S2. (a-c) 3D-AFM images of RT10-HfN films with three film thicknesses of 76 nm (a), 482 nm (b), and 1452 nm (c). (d-f) v_R (d), δ (e) and surface profile (f) of RT10-HfN films.

Table S1. t, d, R, β, the slope of PSD curves at higher frequencies and simulation parameters for RT10-HfN films.

t (min)	d (nm)	Simulation parameters				Simulation			Experiment		
		s (nm)	ds	h (nm)	dh	R (nm)	slope	β	R (nm)	slope	β
5	76	1.6		0.68		0.26	-1.62	0.56	0.26	-1.62	0.56
10	130	2.0	0.25	0.84	0.24	0.34	-1.63		0.35	-1.63	
20	267	4.5	1.81	1.70	1.50	0.46	-2.61		0.46	-2.61	
40	482	7.5	3.69	2.88	3.24	0.75	-3.34		0.75	-3.34	
80	837	12.0	6.50	4.50	5.62	1.13	-3.76		1.13	-3.76	
160	1452	20.0	11.50	7.27	9.69	1.73	-3.92		1.73	-3.92	

Table S2. t, d, R, β, the slope of PSD curves at higher frequencies and simulation parameters for RT40-HfN films.

t (min)	d (nm)	Simulation parameters				Simulation			Experiment		
		s (nm)	ds	h (nm)	dh	R (nm)	slope	β	R (nm)	slope	β
5	47	3.0		1.10		0.35	-2.26	0.63	0.34	-2.26	0.64
10	117	5.1	0.70	2.20	2.00	0.58	-3.23		0.59	-3.23	
20	323	6.4	1.13	3.50	3.18	0.92	-3.49		0.96	-3.49	
40	594	8.0	1.67	5.00	4.55	1.31	-3.58		1.31	-3.58	
80	1032	12.8	3.27	10.12	9.20	2.52	-3.62		2.52	-3.62	
160	1423	14.5	3.83	11.86	10.78	2.92	-3.71		2.93	-3.71	

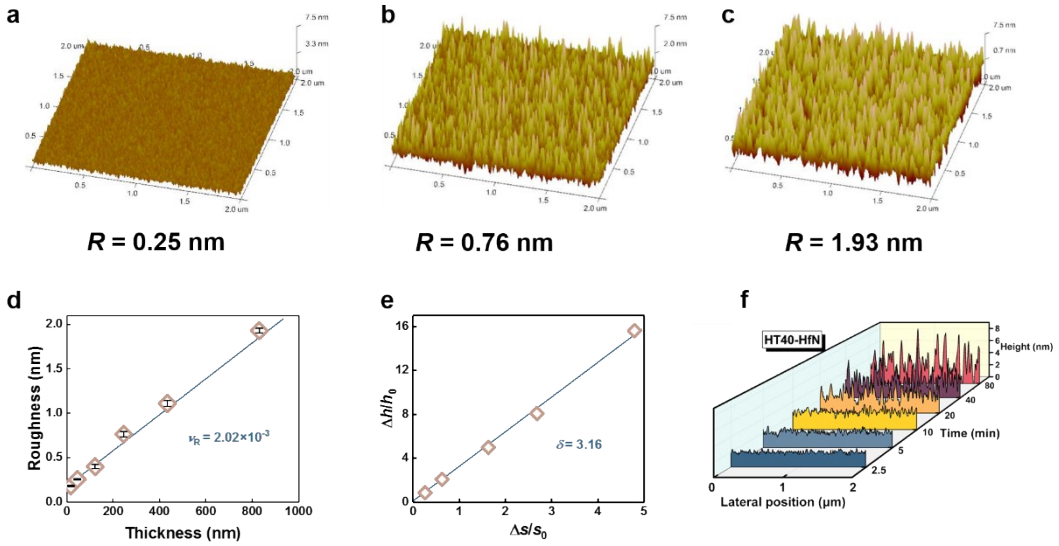

Fig. S3. (a-c) 3D-AFM images of HT40-HfN films with three film thicknesses of 44 nm (a), 245 nm (b) and 830 nm (c). (d-f) ν_R (d), δ (e) and surface profile (f) of HT40-HfN films.

Table S3. t, d, R, β, the slope of PSD curves at higher frequencies and simulation parameters for HT40-HfN films.

t (min)	d (nm)	Simulation parameters				Simulation			Experiment		
		s (nm)	ds	h (nm)	dh	R (nm)	slope	β	R (nm)	slope	β
2.5	~17	1.9		0.46		0.18	-1.46	0.70	0.18	-1.46	0.70
5	44	2.4	0.26	0.85	0.85	0.25	-2.21		0.25	-2.21	
10	122	3.1	0.63	1.42	2.09	0.40	-3.43		0.40	-3.43	
20	245	5.0	1.63	2.75	4.98	0.76	-3.99		0.76	-3.99	
40	434	7.0	2.68	4.17	8.07	1.11	-4.01		1.11	-4.01	
80	830	11.0	4.79	7.64	15.61	1.93	-4.00		1.93	-4.00	

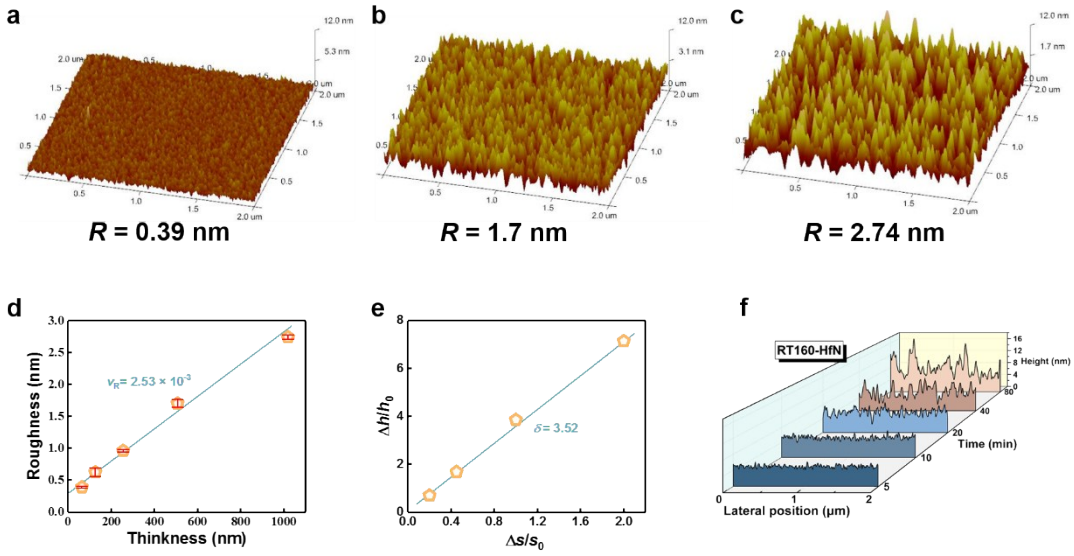

Fig. S4. (a-c) 3D-AFM images of RT160-HfN films with three film thicknesses of 64 nm (a), 507 nm (b) and 1019 nm (c). (d-f) v_R (d), δ (e) and surface profile (f) of RT160-HfN films.

Table S4. *t*, *d*, *R*, *β*, the slope of PSD curves at higher frequencies and simulation parameters for RT160-HfN films.

t (min)	*d* (nm)	Simulation parameters				Simulation			Experiment		
		s (nm)	d*s*	*h* (nm)	d*h*	*R* (nm)	slope	*β*	*R* (nm)	slope	*β*
2.5	~28	2.1		0.79		0.24		0.70	0.24	-2.10	0.70
5	64	2.5	0.19	1.30	0.65	0.39	-3.08		0.39	-3.08	
10	126	3.0	0.43	1.97	1.49	0.62	-3.79		0.62	-3.79	
20	255	4.0	0.90	3.32	3.20	0.96	-3.93		0.96	-3.93	
40	507	6.0	1.86	6.32	7.00	1.71	-3.93		1.70	-3.93	
80	1019	9.5	3.52	10.80	12.67	2.76	-3.93		2.74	-3.93	

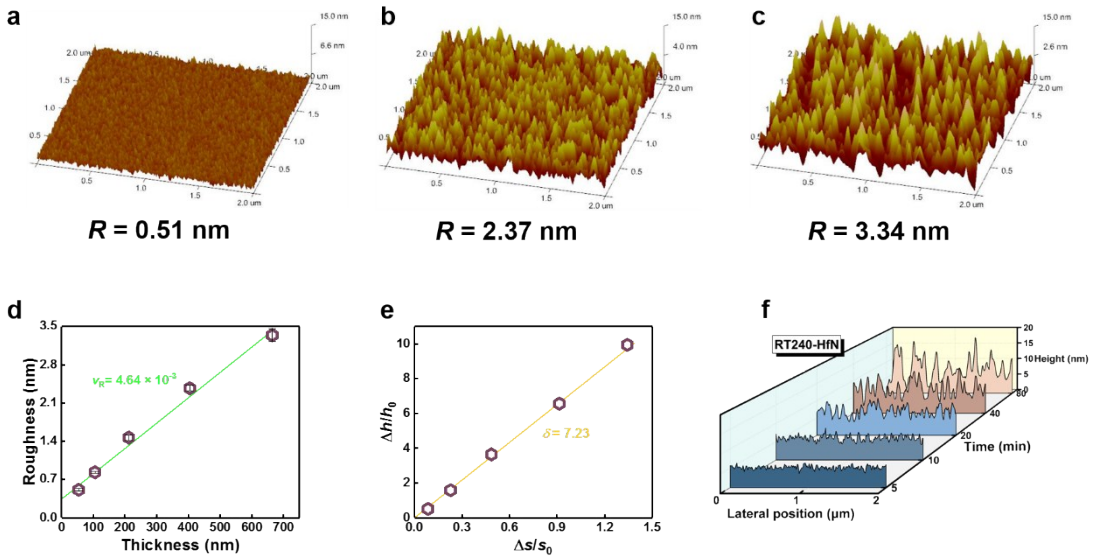

Fig. S5. (a-c) 3D-AFM images of RT240-HfN films with three film thicknesses of 54 nm (a), 404 nm (b) and 664 nm (c). (d-f) ν_R (d), δ (e) and surface profile (f) of RT240-HfN films.

Table S5. *t*, *d*, *R*, *β*, the slope of PSD curves at higher frequencies and simulation parameters for RT240-HfN films.

t (min)	*d* (nm)	Simulation parameters				Simulation			Experiment		
		s (nm)	d*s*	*h* (nm)	d*h*	*R* (nm)	slope	*β*	*R* (nm)	slope	*β*
2.5	~24	3.5		1.19		0.33	-2.19	0.69	0.34	-2.19	0.68
5	54	3.8	0.09	1.80	0.51	0.51	-3.33		0.51	-3.33	
10	105	4.3	0.23	3.08	1.59	0.83	-3.68		0.83	-3.68	
20	212	5.2	0.49	5.53	3.65	1.47	-3.85		1.47	-3.85	
40	404	6.7	0.91	9.00	6.56	2.37	-3.86		2.37	-3.86	
80	664	8.2	1.34	13.02	9.94	3.34	-3.86		3.34	-3.86	

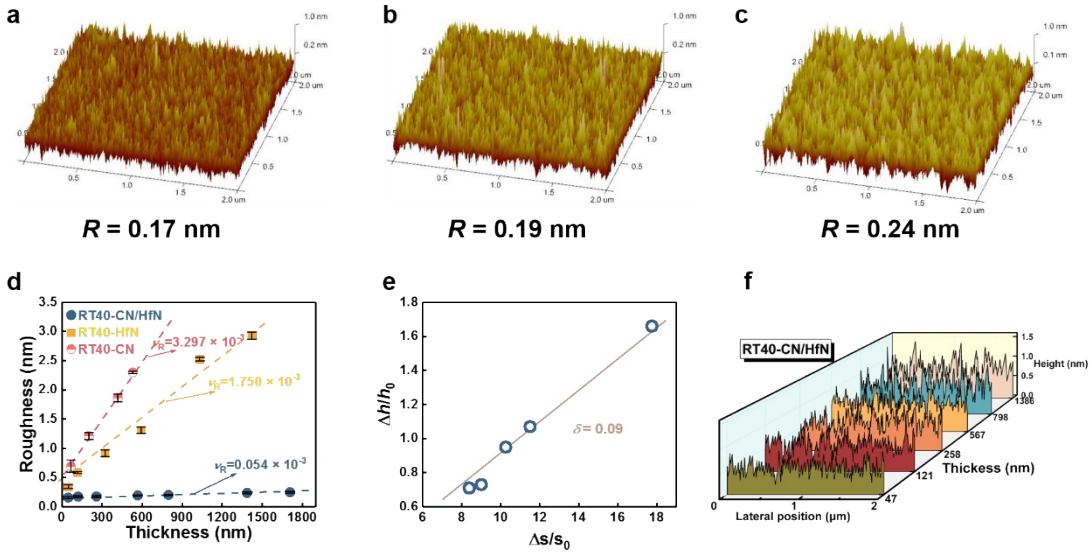

Fig. S6. (a-c) 3D-AFM images of RT40-HfN/CN films with three film thicknesses of 121 nm (a), 567 nm (b) and 1386 nm (c). (d-f) v_R (d), δ (e) and surface profile (f) of RT40-HfN/CN films.

Table S6. t, d, R, β and simulation parameters for RT40-HfN/CN films.

t (min)	d (nm)	Simulation parameters				Simulation		Experiment	
		s (nm)	ds	h (nm)	dh	R (nm)	β	R (nm)	β
20	47	1.6		0.41		0.16	0.13	0.16	0.13
40	121	15.0	8.38	0.70	0.71	0.17		0.17	
80	258	16.0	9.00	0.71	0.73	0.17		0.17	
160	567	18.0	10.25	0.80	0.95	0.19		0.19	
240	798	20.0	11.50	0.85	1.07	0.20		0.20	
480	1386	30.0	17.75	1.09	1.66	0.24		0.24	

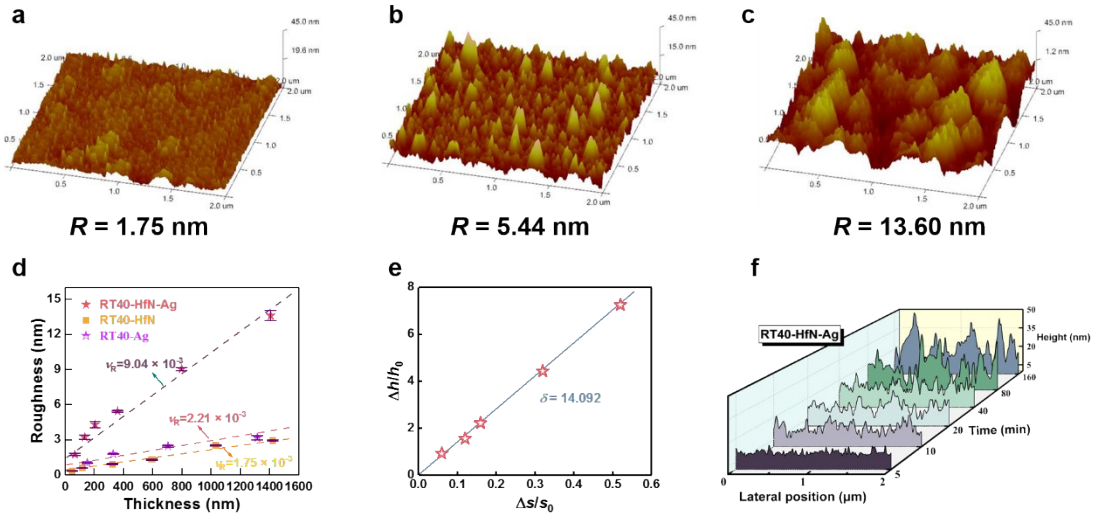

Fig. S7. (a-c) 3D-AFM images of RT40-HfN-Ag films with three film thicknesses of 66 nm (a), 358 nm (b) and 1408 nm (c). (d-f) ν_R (d), δ (e) and surface profile (f) of RT40-HfN-Ag films.

Table S7. t, d, R, β, the slope of PSD curves at higher frequencies and simulation parameters for RT40-HfN-Ag films.

t (min)	d (nm)	Simulation parameters				Simulation			Experiment		
		s (nm)	ds	h (nm)	dh	R (nm)	slope	β	R (nm)	slope	β
5	66	5.0		6.28		1.75	-3.59	0.56	1.75	-3.59	0.56
10	133	5.3	0.06	12.15	0.93	3.22	-3.96		3.22	-3.96	
20	204	5.6	0.12	16.16	1.57	4.30	-3.96		4.30	-3.96	
40	358	5.8	0.16	20.32	2.24	5.44	-3.97		5.44	-3.97	
80	798	6.6	0.32	34.39	4.48	9.04	-3.97		9.03	-3.97	
160	1408	7.6	0.52	52.23	7.32	13.60	-3.97		13.60	-3.97	

Section 3 The GIXRD spectrum for the RT40-HfN/CN film

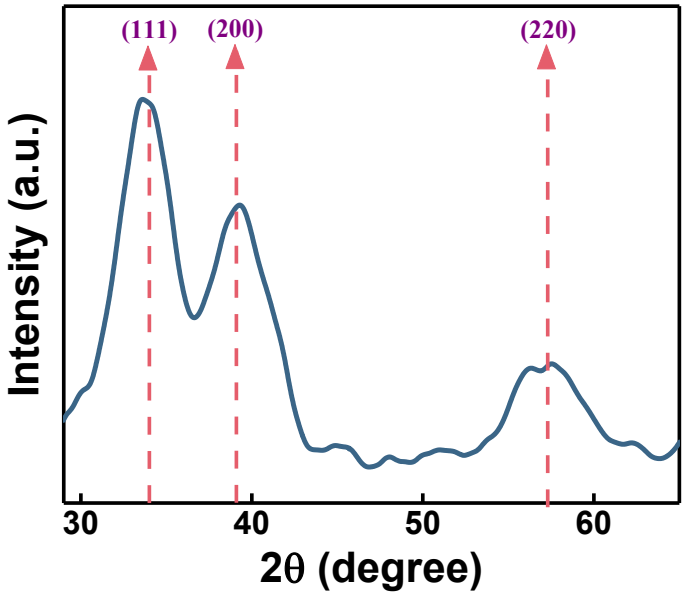

Fig. S8. The GIXRD spectrum for the RT40-HfN/CN film.

Section 4 Hardness and elastic modulus for RT40-HfN, RT40-HfN-Ag and RT40-HfN/CN films

Fig. S9a shows that the hardness of the HfN film increases from 14.8 GPa to 25.3 GPa after Ag doping. Fig. S9b shows that the hardness of the HfN film increases from 14.8 GPa to 24.2 GPa with incorporation of CN layer.

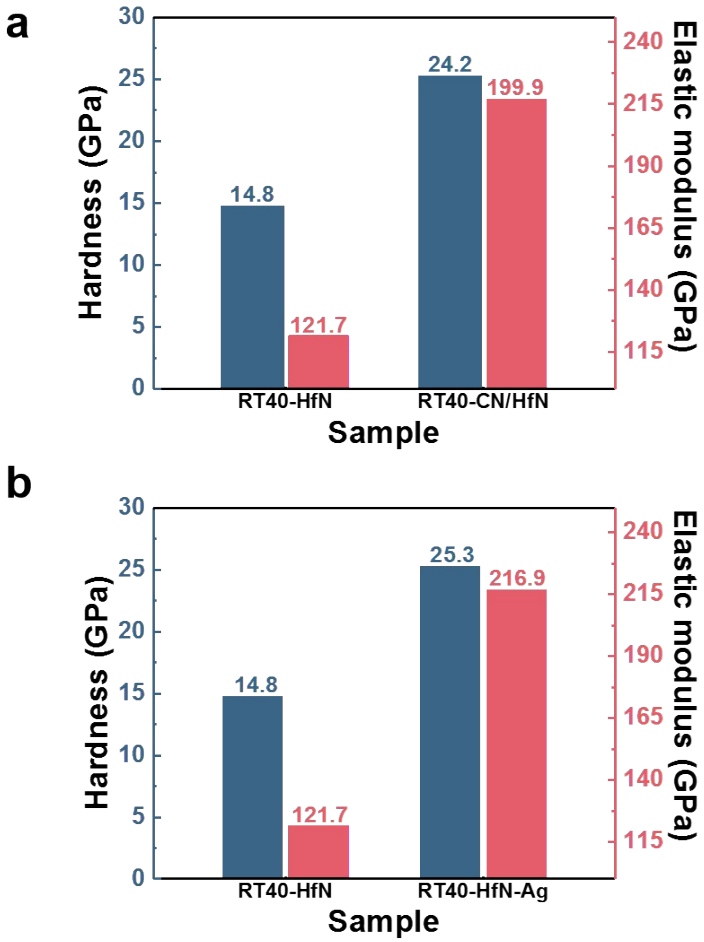

Fig. S9. (a) Hardness and elastic modulus diagram for RT40-HfN and RT40-HfN/CN. (b) Hardness and elastic modulus diagram for RT40-HfN and RT40-HfN-Ag.

Section 5 Water contact angle for RT40-HfN films

We have obtained different surface roughness by changing the film thickness. As the surface roughness of RT40-HfN films increases from 0.92 nm to 2.93 nm, the water contact angle increases from 98.1° to 106.6°.

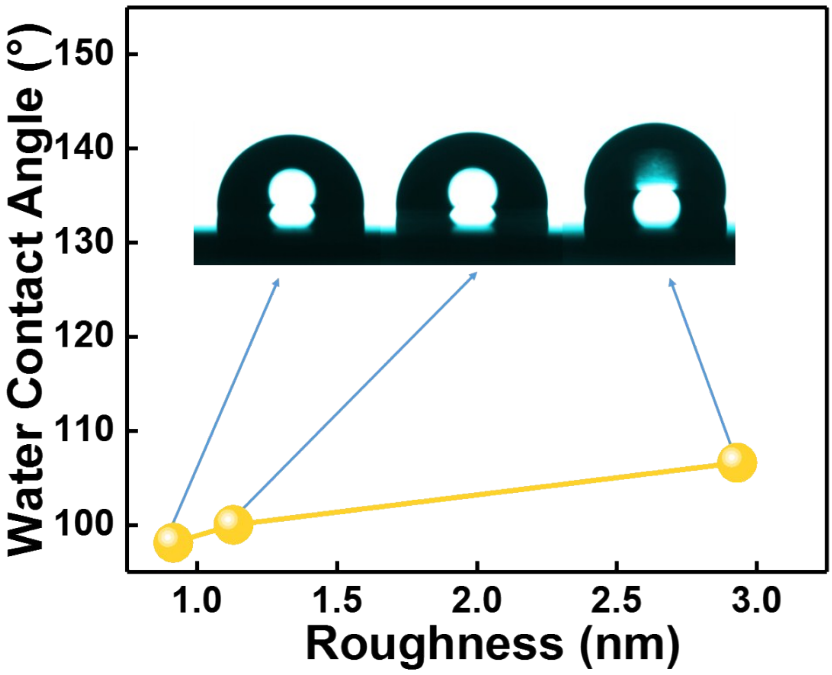

Fig. S10. Water contact angle of RT40-HfN films

Section 6 Wear rate for RT10-HfN, RT40-HfN, RT160-HfN, RT240-HfN, RT40-HfN/CN and RT40-HfN-Ag films

The wear rate of the RT40-HfN film is 5.52×10^{-5} mm^3/Nm. However, the wear rate of the RT40-HfN-Ag film reduces to 4.76×10^{-5} mm^3/Nm, and that of the RT40-HfN/CN film drops to 2.05×10^{-5} mm^3/Nm.

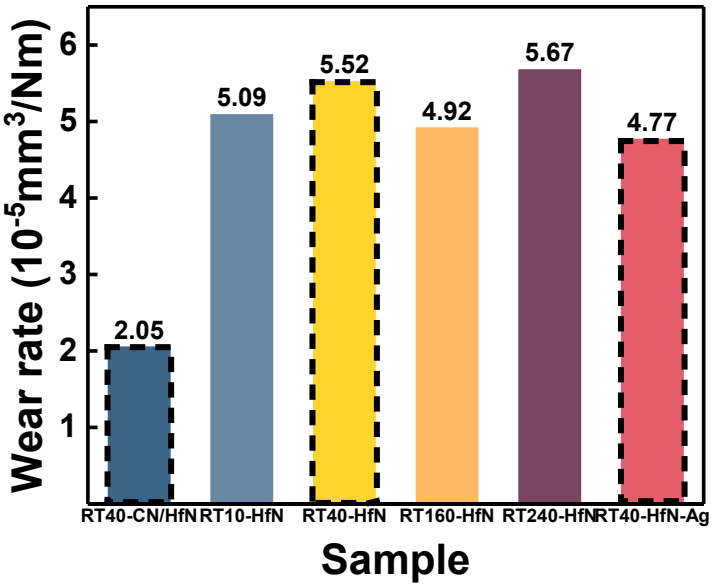

Fig. S11. Wear rate of RT10-HfN, RT40-HfN, RT160-HfN, RT240-HfN, RT40-HfN/CN and RT40-HfN-Ag films with a thickness of approximately 1000 nm.

Section 7 Potentiodynamic polarization curves for RT40-HfN, RT40-HfN-Ag and RT40-HfN/CN films

In a 0.5 mol/L H_2SO_4 electrolyte solution, the corrosion current density of the pure HfN film is 5.09×10^{-4} A·cm^{-2}, the corrosion current density of the Ag-doped HfN film reduces to 5.17×10^{-6} A·cm^{-2}, and the corrosion current density of the HfN/CN multilayer film drops to 2.50×10^{-4} A·cm^{-2}. In a 3.5 wt.% NaCl, the corrosion current density of the pure HfN film is 1.76×10^{-4} A·cm^{-2}, the corrosion current density of the Ag-doped HfN film drops to 4.64×10^{-4} A·cm^{-2}, and the corrosion current density of the HfN/CN multilayer film reduces to 8.17×10^{-5} A·cm^{-2}.

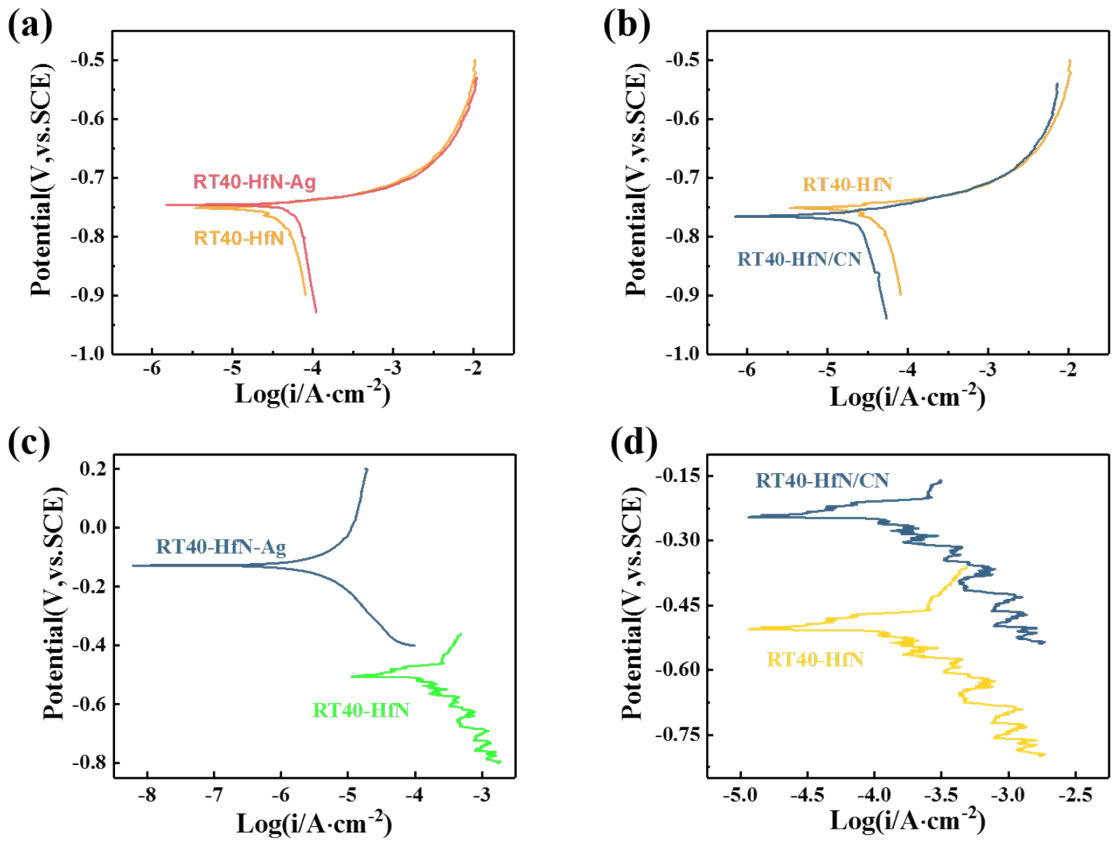

Fig. S12. (a and b) Potentiodynamic polarization curves of RT40-HfN (a), RT40-HfN-Ag (a), RT40-HfN/CN films (b) in salt environment. (c and d) Potentiodynamic polarization curves of RT40-HfN (c), RT40-HfN-Ag (c) and RT40-HfN/CN films (d) in acid environment.

Section 8 Optical micrographs of the wear tracks for RT40-HfN, RT40-HfN/CN and RT40-HfN-Ag films

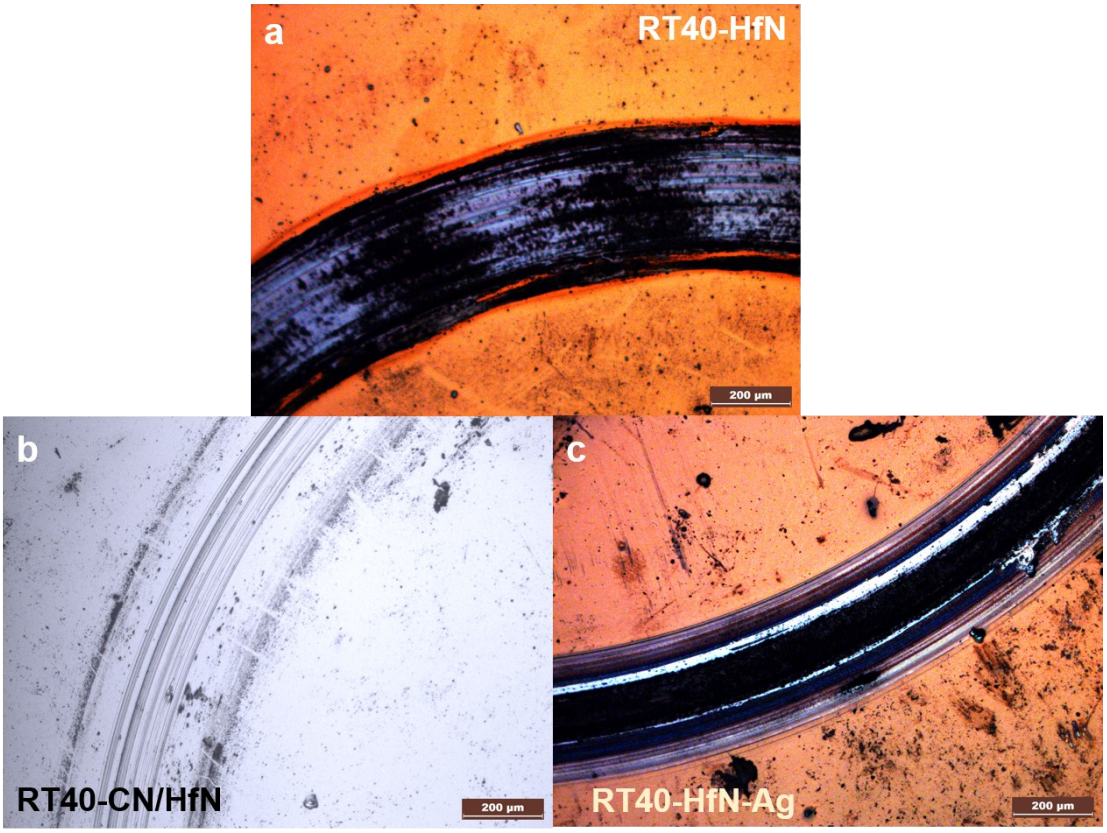

Fig. S13. Optical micrographs of the wear tracks for RT40-HfN (a), RT40-HfN/CN (b) and RT40-HfN-Ag films (c).

Section 9 v_R, δ, surface topography and simulation details for Ag films, including Figure S14-S18 and Table S8-S11.

To verify the universality of the model, we prepared Ag films under different bias conditions. The specific implementation details are the same as described in the section 2. According to Fig. S14-S17, we can see that the Ag films also have surface roughening behavior. To demonstrate the reliability of our model, the dependency relationship between v_R and δ was plotted (Fig. S18). v_R is in good linear relationship with δ, where $k = 3.32\times10^{-4}$. These results clearly prove that the roughening rate of the film is indeed proportional to the relative vertical-growth coefficient of mounds, and this model is also applicable to metal-bonding materials.

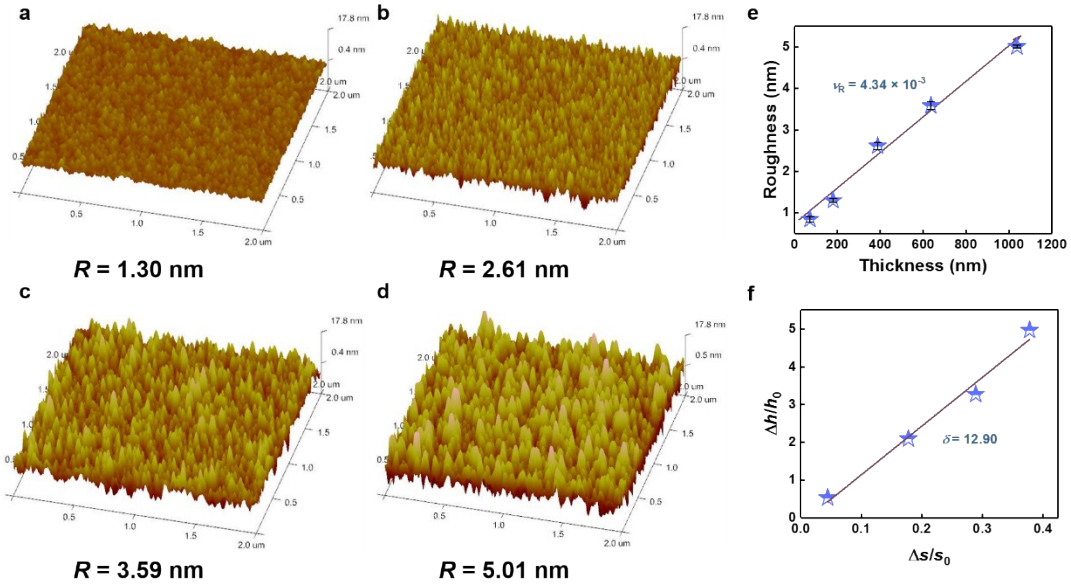

Fig. S14. (a-d) 3D-AFM images of Ag films with four film thicknesses of 179nm (a), 387 nm (b), 635 nm (c) and 1036 nm (d). (e and f) v_R (e) and δ (f) of RT-floating-Ag films.

Table S8. t, d, R, β, the slope of PSD curves at higher frequencies and simulation parameters for RT-floating-Ag films.

t (min)	d (nm)	Simulation parameters				Simulation			Experiment		
		s (nm)	ds	h (nm)	dh	R (nm)	slope	β	R (nm)	slope	β
5	71	4.5		2.66		0.85	-3.16	0.66	0.85	-3.15	0.66
10	179	4.7	0.04	4.08	0.53	1.30	-3.24		1.30	-3.26	
20	387	5.3	0.18	8.23	2.09	2.61	-3.36		2.61	-3.34	
40	635	5.8	0.29	11.36	3.27	3.59	-3.64		3.59	-3.66	
80	1036	6.2	0.38	15.88	4.97	5.01	-3.94		5.01	-3.92	

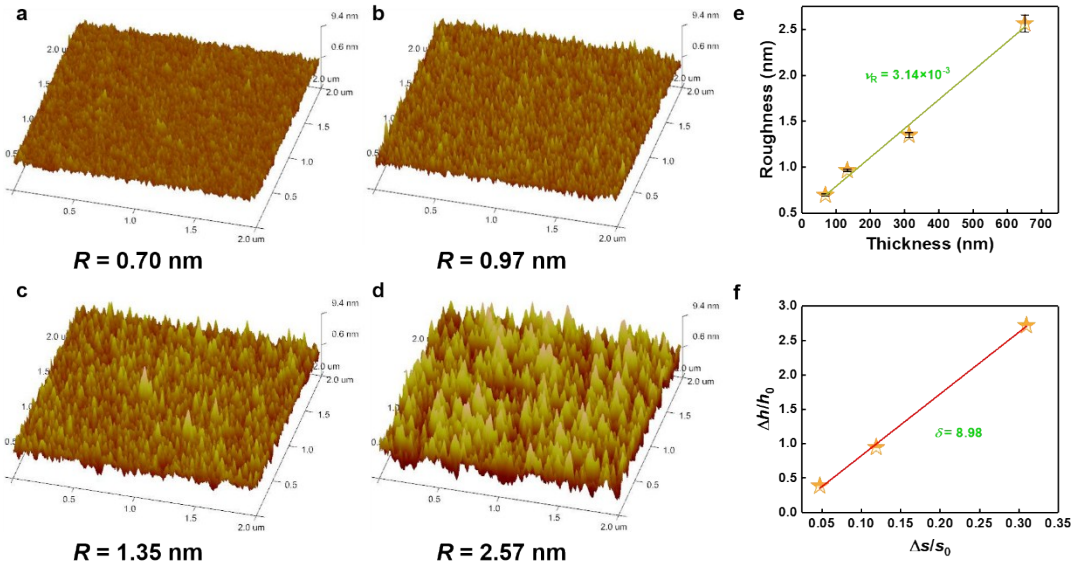

Fig. S15. (a-d) 3D-AFM images of Ag films with four film thicknesses of 68 nm (a), 132 nm (b), 313 nm (c) and 651 nm (d). (e and f) ν_R (e) and δ (f) of RT10-Ag films.

Table S9. t, d, R, β, the slope of PSD curves at higher frequencies and simulation parameters for RT10-Ag films.

t (min)	d (nm)	Simulation parameters				Simulation			Experiment		
		s (nm)	ds	h (nm)	dh	R (nm)	slope	β	R (nm)	slope	β
5	68	4.2		2.18		0.70	-3.35	0.61	0.70	-3.32	0.61
10	132	4.4	0.05	3.03	0.39	0.97	-3.46		0.97	-3.45	
20	313	4.7	0.12	4.25	0.95	1.35	-3.66		1.35	-3.66	
40	651	5.5	0.31	8.11	2.72	2.57	-3.61		2.57	-3.61	

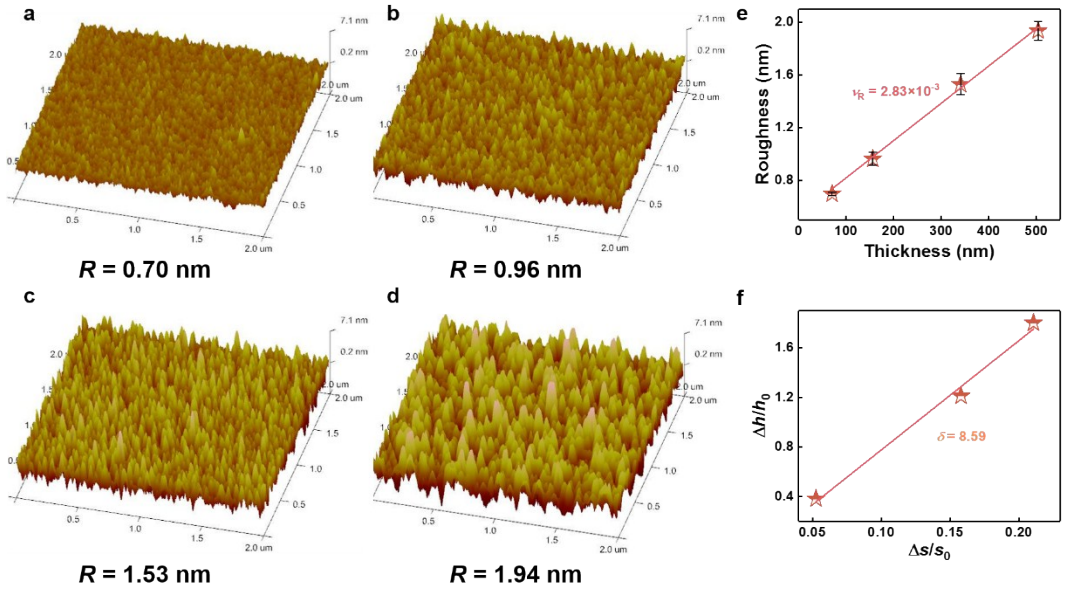

Fig. S16. (a-d) 3D-AFM images of Ag films with four film thicknesses of 70 nm (a), 158 nm (b), 340 nm (c) and 503 nm (d). (e and f) v_R (e) and δ (f) of RT20-Ag films.

Table S10. *t*, *d*, *R*, *β*, the slope of PSD curves at higher frequencies and simulation parameters for RT20-Ag films.

t (min)	*d* (nm)	Simulation parameters				Simulation			Experiment		
		s (nm)	d*s*	*h* (nm)	d*h*	*R* (nm)	slope	*β*	*R* (nm)	slope	*β*
5	70	3.8		2.17		0.70	-3.12	0.51	0.70	-3.13	0.51
10	155	4.0	0.05	3.00	0.38	0.96	-3.16		0.96	-3.17	
20	340	4.4	0.16	4.80	1.21	1.53	-3.15		1.53	-3.16	
40	503	4.6	0.21	6.08	1.80	1.94	-3.35		1.94	-3.33	

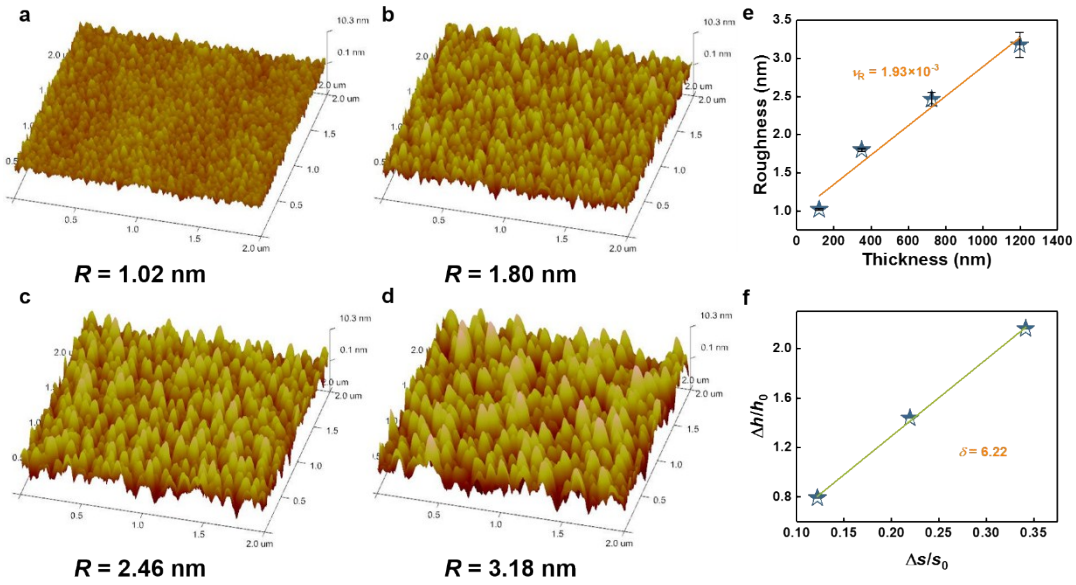

Fig. S17. (a-d) 3D-AFM images of Ag films with four film thicknesses of 121 nm (a), 349 nm (b), 725 nm (c) and 1197 nm (d). (e and f) v_R (e) and δ (f) of RT40-Ag films.

Table S11. *t*, *d*, *R*, *β*, the slope of PSD curves at higher frequencies and simulation parameters for RT40-Ag films.

t (min)	*d* (nm)	Simulation parameters				Simulation			Experiment		
		s (nm)	d*s*	*h* (nm)	d*h*	*R* (nm)	slope	*β*	*R* (nm)	slope	*β*
5	121	4.1		3.18		1.02	-3.71	0.54	1.02	-3.71	0.54
10	349	4.6	0.12	5.70	0.79	1.80	-3.78		1.80	-3.77	
20	725	5.0	0.22	7.75	1.44	2.46	-3.88		2.46	-3.88	
40	1197	5.5	0.34	10.05	2.16	3.18	-3.96		3.18	-3.96	

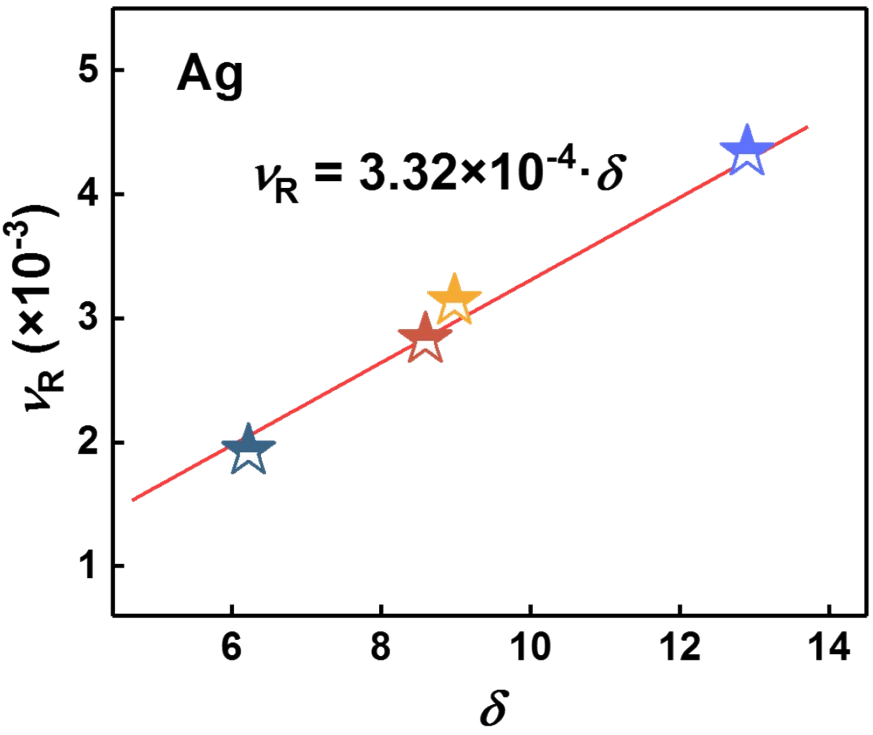

Fig. S18. The proportional relationship between v_R and δ of Ag films, where k is equal to 3.32×10^{-4}.

Section 10 v_R, δ, surface topography and simulation details for HfO_2 films, including figure S19-S23 and table S12-S15.

To verify the universality of the model, we prepared HfO_2 films under different bias conditions. The specific implementation details are also the same as described in the section 2. According to Fig. S19-S22, we can see that the HfO_2 films also have surface roughening behavior. To demonstrate the reliability of our model, the dependency relationship between v_R and δ was plotted (Fig. S23). v_R is in good linear relationship with δ, where $k = 5.23\times10^{-4}$. These results clearly prove that the roughening rate of the film is indeed proportional to the relative vertical-growth coefficient of mounds, and this model is also applicable to ionic-bonding materials.

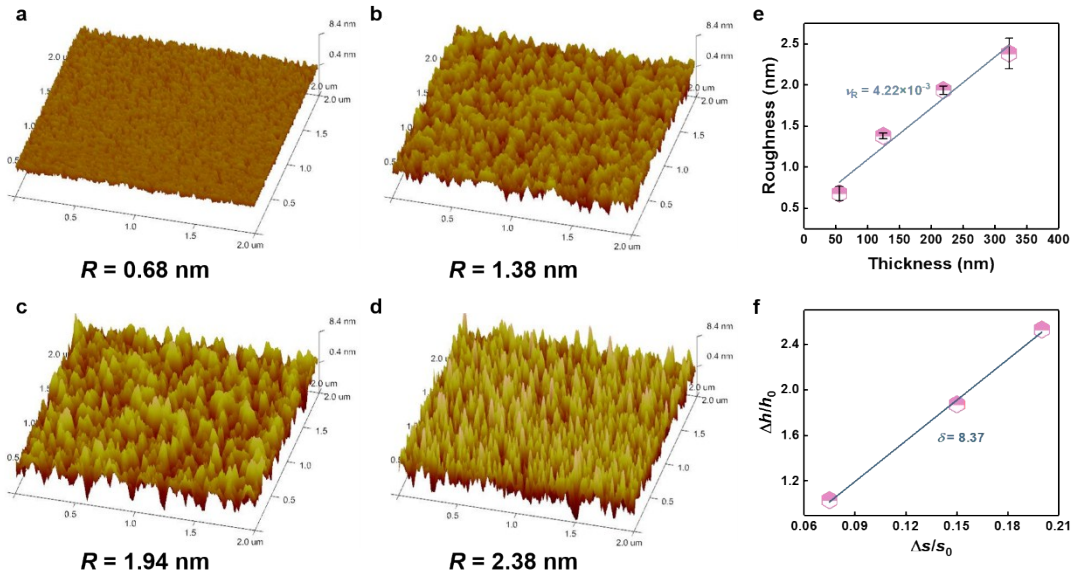

Fig. S19. (a-d) 3D-AFM images of HfO_2 films with four film thicknesses of 55 nm (a), 124 nm (b), 218 nm (c) and 321 nm (d). (e and f) v_R (e) and δ (f) of RT-floating-HfO_2 films.

Table S12. *t*, *d*, *R*, *β*, the slope of PSD curves at higher frequencies and simulation parameters for RT-floating-HfO_2 films.

t (min)	*d* (nm)	Simulation parameters				Simulation			Experiment		
		s (nm)	d*s*	*h* (nm)	d*h*	*R* (nm)	slope	*β*	*R* (nm)	slope	*β*
10	55	4.0		2.12		0.68	-3.04	0.59	0.68	-3.03	0.59
20	124	4.3	0.08	4.31	1.03	1.38	-2.98		1.38	-3.00	
40	218	4.6	0.15	6.09	1.87	1.94	-2.90		1.94	-2.91	
80	321	4.8	0.20	7.48	2.53	2.38	-3.55		2.38	-3.58	

.

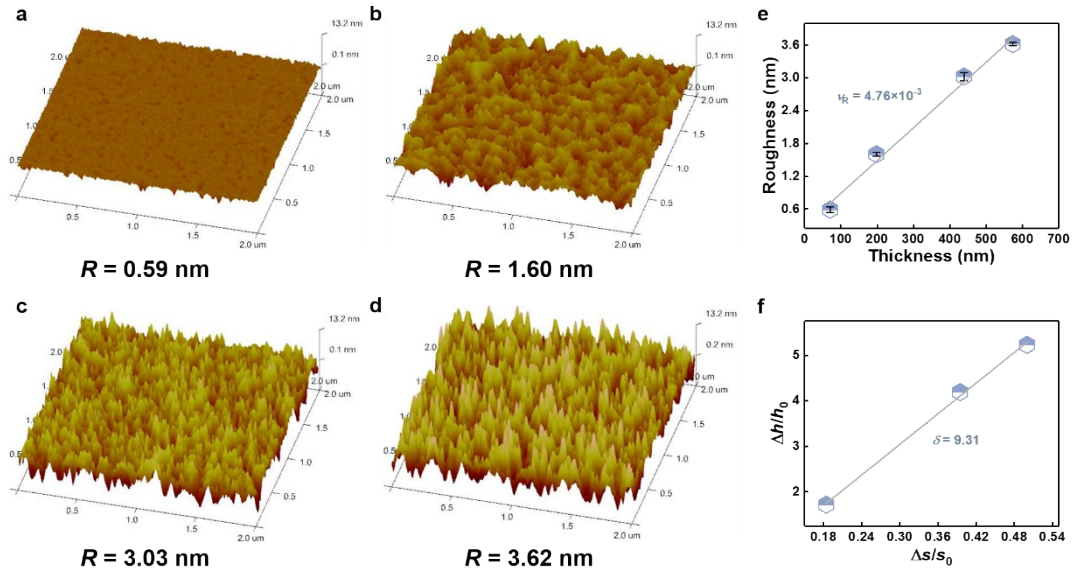

Fig. S20. (a-d) 3D-AFM images of HfO_2 films with four film thicknesses of 70 nm (a), 108 nm (b), 438 nm (c) and 573 nm (d). (e and f) ν_R (e) and δ (f) of RT20-HfO_2 films.

Table S13. *t*, *d*, *R*, *β*, the slope of PSD curves at higher frequencies and simulation parameters for RT20-HfO_2 films.

t (min)	*d* (nm)	Simulation parameters				Simulation			Experiment		
		s (nm)	*ds*	*h* (nm)	d*h*	*R* (nm)	slope	*β*	*R* (nm)	slope	*β*
10	70	3.8		1.84		0.59	-3.23	0.88	0.59	-3.23	0.88
20	198	4.5	0.18	5.00	1.72	1.60	-3.26		1.60	-3.23	
40	438	5.3	0.39	9.55	4.19	3.03	-4.09		3.03	-4.08	
80	573	5.7	0.50	11.46	5.23	3.62	-4.09		3.62	-4.11	

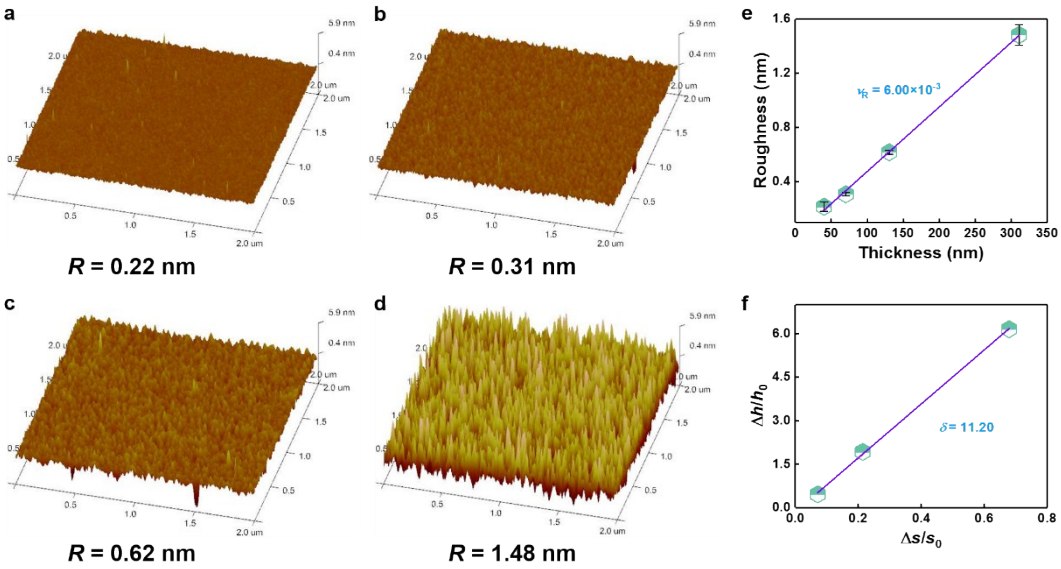

Fig. S21. (a-d) 3D-AFM images of HfO_2 films with four film thicknesses of 40 nm (a), 65 nm (b), 141 nm (c) and 305 nm (d), respectively. (e and f) v_R (e) and δ (f) of RT40-HfO_2 films.

Table S14. *t*, *d*, *R*, *β*, the slope of PSD curves at higher frequencies and simulation parameters for RT40-HfO_2 films.

t (min)	*d* (nm)	Simulation parameters				Simulation			Experiment		
		s (nm)	d*s*	*h* (nm)	d*h*	*R* (nm)	slope	*β*	*R* (nm)	slope	*β*
5	~40	2.8		0.65		0.22	-1.84	0.93	0.22	-1.83	0.93
10	65	3.0	0.07	0.95	0.46	0.31	-2.84		0.31	-2.85	
20	141	3.4	0.21	1.90	1.92	0.62	-3.57		0.62	-3.59	
40	315	4.7	0.68	4.65	6.15	1.48	-3.63		1.48	-3.63	

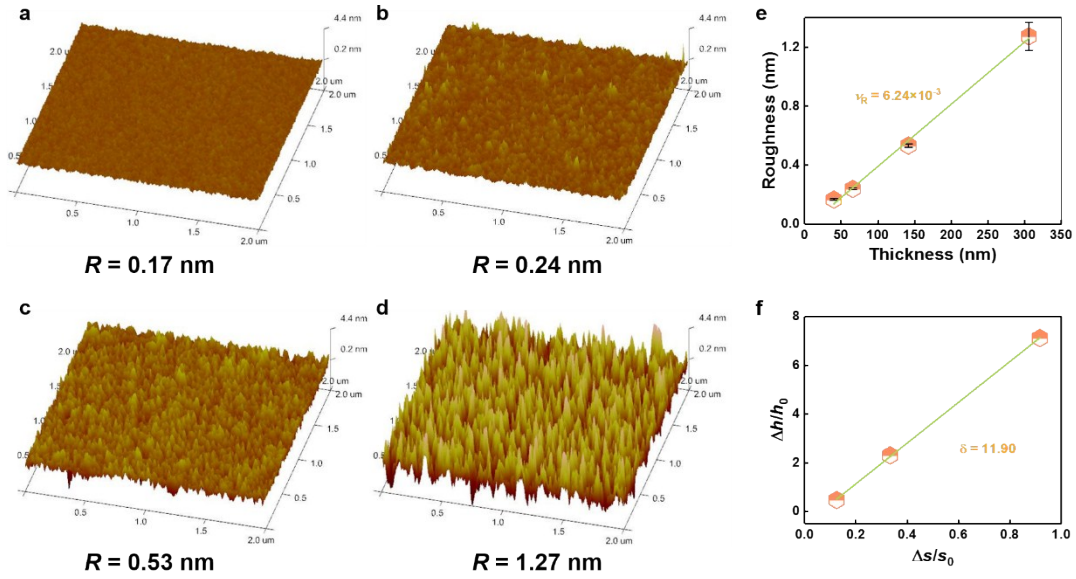

Fig. S22. (a-d) 3D-AFM images of HfO_2 films with four film thicknesses of 40 nm (a), 70 nm (b), 130 nm (c) and 310 nm (d). (e and f) v_R (e) and δ (f) of RT60-HfO_2 films.

Table S15. *t*, *d*, *R*, *β*, the slope of PSD curves at higher frequencies and simulation parameters for RT60-HfO_2 films.

t (min)	*d* (nm)	Simulation parameters				Simulation			Experiment		
		s (nm)	d*s*	*h* (nm)	d*h*	*R* (nm)	slope	*β*	*R* (nm)	slope	*β*
5	~40	2.4		0.49		0.17	-1.14	0.98	0.17	-1.15	0.98
10	70	2.7	0.13	0.72	0.47	0.24	-2.12		0.24	-2.15	
20	130	3.2	0.33	1.62	2.31	0.53	-2.76		0.53	-2.75	
40	310	4.6	0.92	3.98	7.12	1.27	-2.85		1.27	-2.82	

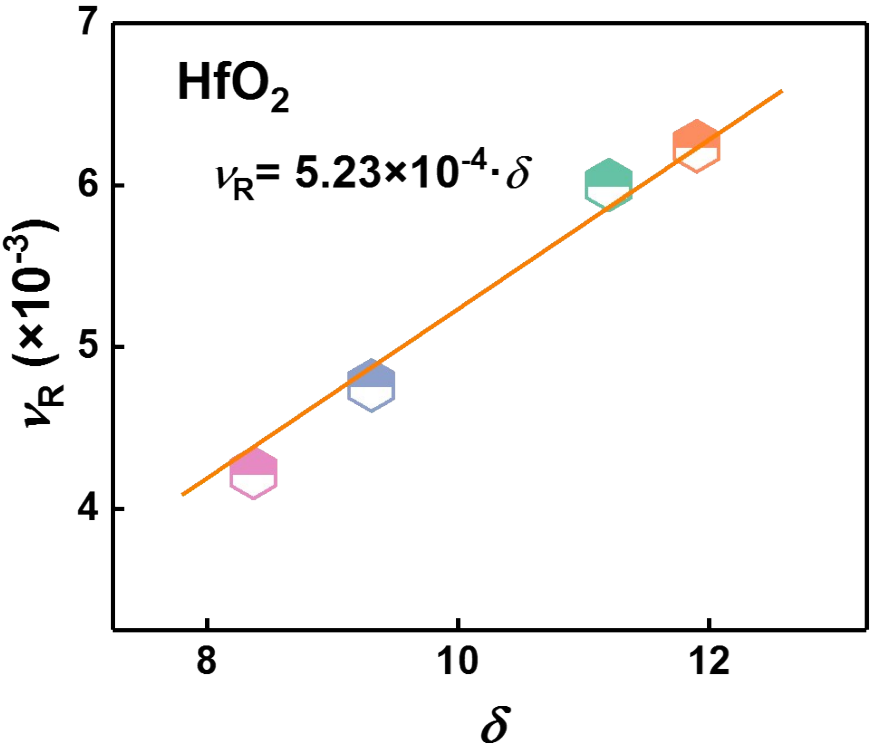

Fig. S23. The proportional relationship between v_R and δ of HfO_2 films, where k is equal to 5.23×10^{-4}.

Section 11 Thickness and roughness of HfN films under different growth conditions

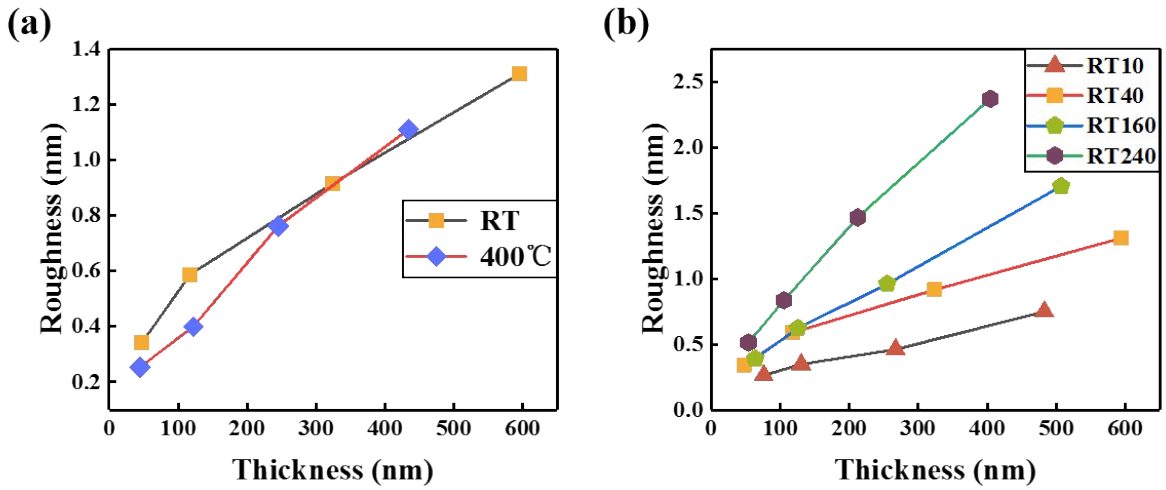

Fig. S24. (a) The surface roughness of HfN films prepared at varying substrate temperature (room temperature and 400 ℃) as a function of thickness. (b) The surface roughness of HfN films prepared at varying substrate bias (-10 V, -40 V, -160 V and -240 V) as a function of thickness.

Section 12 Simulation steps

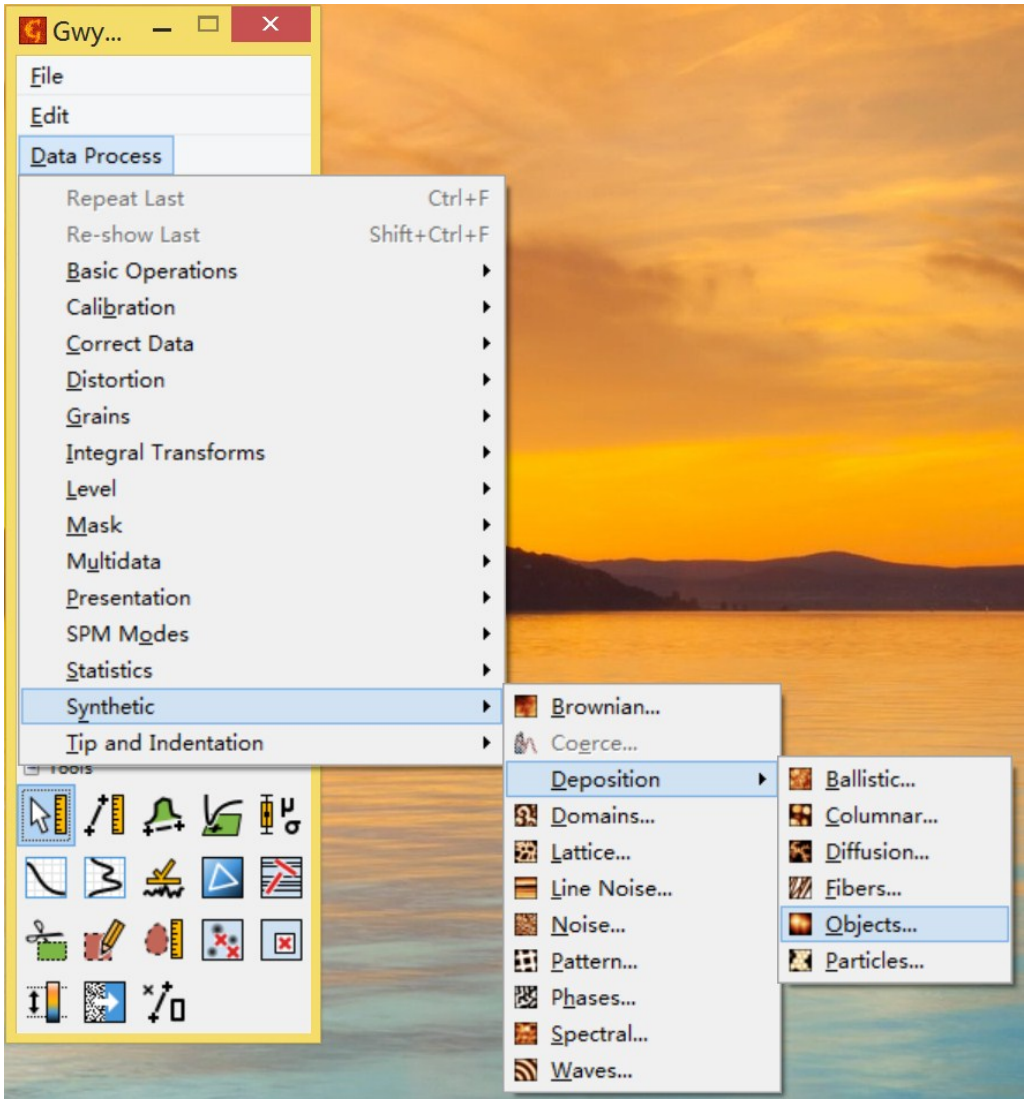

Fig. S25. Choosing the simulation mode.

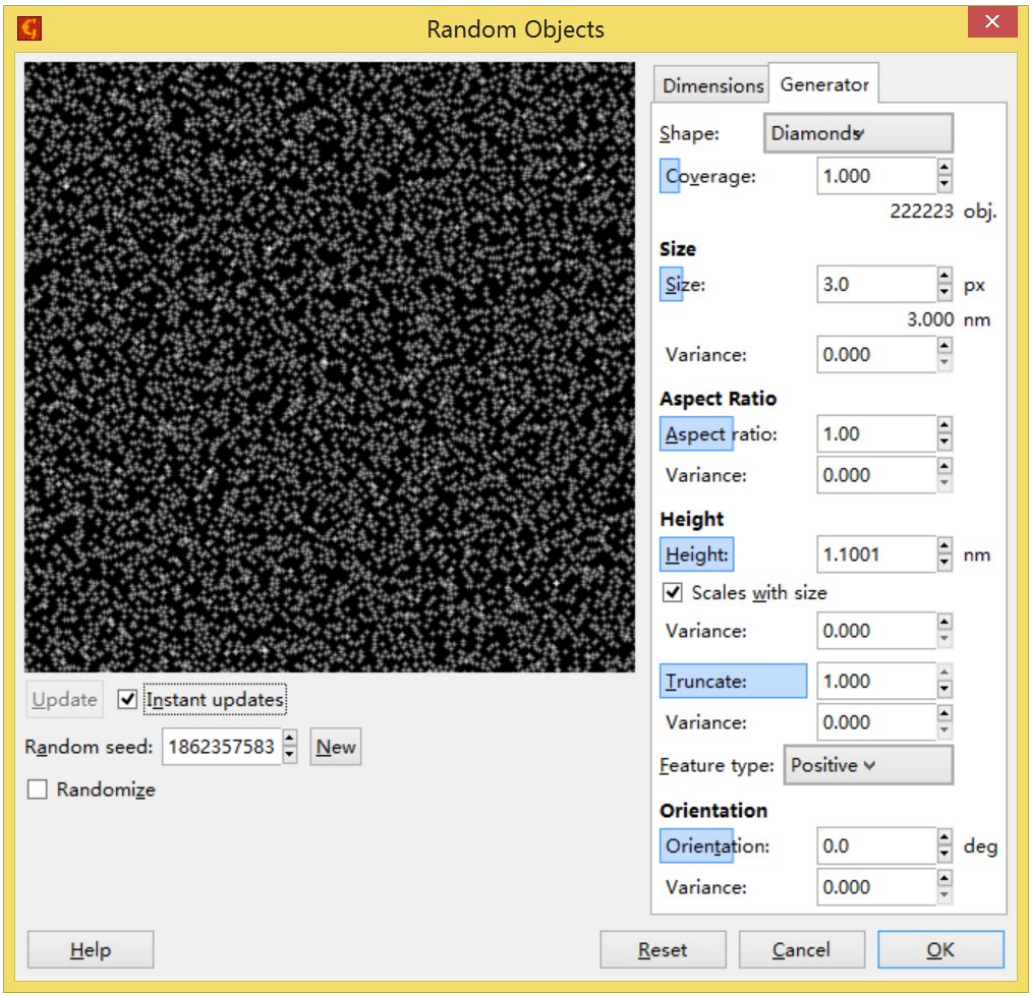

Fig. S26. Setting the simulation parameters.